Available online at www.sciencedirect.com

ScienceDirect

Procedia Computer Science 168 (2020) 3–10

Procedia Computer Science

www.elsevier.com/locate/procedia

Complex Adaptive Systems Conference with Theme:
Leveraging AI and Machine Learning for Societal Challenges, CAS 2019

Machine Learning for Attribution of Heat and Drought in Southwestern Australia

Michael B. Richman[a]* and Lance M. Leslie[b]

[a] School of Meteorology, University of Oklahoma,120 David L. Boren Blvd, Suite 5600, Norman, OK, 73072 USA
[b]School of Mathematical and Physical Science, University of Technology Sydney, 15 Broadway, Ultimo, NSW 2007, Australia

Abstract

Temperature and precipitation datasets, extending back over 100 years, are analyzed at Perth, Australia. Observational analyses reveal the emergence of hot and dry years since the 1980s, with changes in maximum temperatures ~1.5-2 °C above historical means. These temperatures far exceed recorded natural variability measured in the early 20th century and, in the past few decades, have accelerated above the danger threshold established in the Paris Accords. Permutation testing of mean Perth temperature (precipitation) for the 20-year periods 1979-1998 and 1999-2018 shows an increase (decrease) of 0.855 °C (98.1 mm); p-value 0.001 (0.0087). Attribution of interannual data variability is established by wavelet analyses. Linear and support vector regression (LR, SVR), neural network (NN) and random forests (RF) are used for temperature and precipitation prediction after attribute selection methods are applied to a set of climate drivers. Forecasts on independent testing data show that for temperature and precipitation forecasts, SVR, LR and NN (temperature only) provide more accurate predictions than RF. The features selected by attribute selection and machine learning provide important guidance for climate forecasting, policy planning and management.

Peer-review under responsibility of the scientific committee of the Complex Adaptive Systems Conference with Theme: Leveraging AI and Machine Learning for Societal Challenges

Keywords: Machine learning; Heat and drought; Attribution; Prediction; Southwestern Australia

1. Introduction

The definition of drought has evolved from its simple meteorological definition as a regional rainfall deficit that occurs over a period of time. The actual deficit and time period vary greatly with the geographical location of the region. This limited definition of drought has since diversified into five stages of drought that occur sequentially. Meteorological drought is followed by hydrological

* Corresponding author. Tel.: +1-405-325-1853; fax: +1-405-325-7689.
E-mail address: mrichman@ou.edu

Peer-review under responsibility of the scientific committee of the Complex Adaptive Systems Conference with Theme: Leveraging AI and Machine Learning for Societal Challenges
10.1016/j.procs.2020.02.244

drought, which is present when decreases in river and stream flows, along with ground water, cause water storages to fall below pre-defined critical levels. Next is agricultural drought, which occurs when soil moisture is insufficient to maintain necessary crop production. Ecological drought follows, and is the damage, often catastrophic, resulting from soil moisture levels falling so low that the fundamental ecology of a region is no longer sustainable. The final stage is socio-economic drought, which is a failure of the supply of crops and other products to meet the public need. Socio-economic drought is, in many countries, the most catastrophic kind of natural disaster. The socio-economic drought Cape Town [1] provides a precautionary study for Perth, Australia, which lies at a similar latitude and also has a Mediterranean climate. Just as the Cape Town and California droughts were exacerbated by increasing temperatures the mean maximum temperatures in this southwestern Australian city also have been observed to increase, particularly since the 1970s. Increasing temperatures typically lead to additional stress on water resources, including increased evaporation of water and enhanced risk of bushfires Population has also been increasing, requiring a concomitant increase in water supply.

The goals of this work are (1) to quantitatively document the severity of the aforementioned Perth water crisis using permutation resampling techniques, and (2) to attribute the components of drought by examining the relative roles of long-term climate change versus cyclical climate drivers by using a variety of statistical and machine learning methods to predict temperature and rainfall for the past 37 years. Both goals are important for water management.

2. Data and Methods

2.1. Data

The monthly time series of precipitation and maximum temperatures (Tmax) were obtained for Perth (Fig. 1) from the publicly available Climate Data Online section of the Australian Bureau of Meteorology (BoM) website (http://www.bom.gov.au/climate/data/index.shtml). The wet season for each city was determined simply by computing the monthly averages of precipitation, over the entire length of the time series data, and then comparing various monthly subsets with the remaining months. For Perth, the wet season was found to roughly

Fig. 1. Map of Australia, showing location of Perth.

coincide with the “southern wet season" as defined by the Bureau of Meteorology (www.bom.gov.au) to be April to November, inclusive.

The climate drivers consist of the global temperature time series obtained from NASA for the years 1910-2018 (https://data.giss.nasa.gov/gistemp/) and a set of climate indices, i.e., Dipole Mode Index (DMI, Southern Oscillation Index, (SOI) Niño 3, Niño 4, Pacific Decadal Oscillation (PDO), Antarctic Oscillation (AAO), Atlantic Meridional Oscillation (AMO), North Pacific Index (NPI) , Interdecadal Pacific Oscillation (IPO), obtained from the Earth System Research Laboratory, for the same range of years (https://www.esrl.noaa.gov/psd/gcos_wgsp/Timeseries/). The cross-products between the aforementioned climate drivers were calculated and served as additional potential attributes.

2.2. Methods and preprocessing

For the assessment of climate change, permutation testing of mean precipitation differences between the 20-year periods 1979-1998 and 1999-2018 was employed to obtain the significance level of change. The attribution work employed a set of four techniques that are suited to predicting numeric values: linear regression (LR) [2], support vector regression (SVR) [3], a feedforward neural network (NN) [4] and a random forest (RF) [5]. Data for the years 1910-1981 were used to select attributes (the training data). The prediction accuracy of each of the attribution techniques is dependent upon selecting those attributes which generalize well. As

there exists no single method to determine the best set of attributes for a given technique, a range of attribute selection techniques were applied for both temperature (Table 1) and precipitation (Table 2). The techniques applied were a correlation-based feature selection with greedy hill climbing, augmented with a backtracking facility (CfsBF) [6], wrapper subset evaluation [7] using various classifiers: linear regression (LRBF), a backpropagation neural network (NNBF), support vector regression (SVRBF) and a random forest (RFBF). A second group of techniques used classifier subset selection [8] with each of the aforementioned classifiers (LRCS; NNCS; SVRCS; RFCS). The final attribute evaluator was a classifier subset selection using the aforementioned evaluators with a greedy forward search though the space of attribute subsets [9] (LRGr; NNGr; SVRGr; RFGr). The precipitation analysis (Table 2) used the same feature selection techniques, with sea surface temperature anomalies near Perth added as an additional potential attribute.

Using resampling, via a 10-fold cross-validation on the training data, preprocessing for temperature (Table 1) revealed that the global temperature data set and DMI were the leading predictors selected among feature selection methods with means of 100 and 62.3 percent of the folds containing these climate drivers. However, other drivers emerged in the majority of folds for specific techniques (e.g., Niño4 for LR). Those features were passed on for further analysis. The last column shows the mean of the number of folds, a good indication of the appropriateness of each attribute. For the precipitation features (Table 2), the leading climate drivers were AAO and SOI, respectively. Once again, specific techniques had other climate drivers in the majority of folds (e.g., IPO for SVR). A comparison of the similarities among the feature techniques is summarized in the dendrogram of an average linkage cluster analysis (Fig. 2). For the selection of temperature variables, Fig. 2 shows that the wrapper and greedy forward search though the space of attribute subsets often are closely clustered whereas, for precipitation, this is not the case and the LR and RF methods are closely clustered. The last column is the mean number of attribute folds.

Linear regression (LR), neural networks (NN), support vector regression (SVR) and random forests (RF) were used to predict the temperature and precipitation in Perth for the years 1982-2018 (the testing data), those attributes that were present in at least 5 of 10 folds were passed to the prediction techniques for further winnowing.

3. Results

3.1. Drought assessment

Increasing average maximum temperatures imply increased evaporation, strengthening the effects of decreasing wet season precipitation. As such, it is important to understand how temperatures have changed over that period. Fig. 3 shows the time series of maximum temperatures (Tmax) for Perth, over the southern wet season. An obvious feature is the striking increase in Tmax since 1910, with increased in the warming rate since the 1970s. In the past decade, no year was below the median and only one year below the 75th percentile. The precipitation data (Fig. 3) show roughly the reverse pattern, where the decrease is most notable since the 1950s. Most years in the past decade have been in the historical 10th to 25th percentiles. The combination of extreme warmth and meager precipitation is similar to that found globally in other Mediterranean climates, such as southern California and Cape Town, South Africa.

Owing to the large year-to-year variability in the annual values of Tmax and precipitation, individual years in 20- year subsets, 5000 bootstrap replicates of the mean for each 20-year period were calculated. Boxplots of those means are shown (Fig. 4) for both Tmax and precipitation. The boxplots for Tmax show, for subsequent 20-year

Table 1. Attribute selection for 13 different methods for maximum temperature prediction in Perth. The percent of folds selecting the attribute is shown for each of the 13 methods (columns 2-14). Statistics (mean, standard deviation, skewness and kurtosis) for each column are shown.

Attribute /Method	Cfs BF	LR BF	NN BF	SVR BF	RF BF	LR CS	NN CS	SVR CS	RF CS	LR Gr	NN Gr	SVR Gr	RF Gr	Mean
Global T	100	100	100	100	100	100	100	100	100	100	100	100	100	100
NPI	0	0	0	30	70	10	90	70	90	0	0	30	70	35.4
IPO	0	20	0	10	0	100	40	90	0	10	0	10	0	21.5
Niño3	0	0	10	10	0	10	50	90	0	0	0	0	0	13.1
Niño4	0	60	20	10	0	100	70	90	0	50	20	20	10	34.6
SOI	0	0	10	40	0	60	60	60	0	0	0	20	0	19.2
AMO	0	20	20	0	80	40	100	80	50	20	10	10	70	38.5
PDO	0	30	30	60	10	90	80	80	0	30	30	50	10	39.2
DMI	80	80	50	90	20	90	70	100	20	80	30	90	20	63.1
AAO	0	10	40	80	0	20	40	60	100	10	30	50	0	33.8
GTxNiño3	0	0	0	0	10	10	60	100	20	0	0	0	10	16.2

GTxNiño4	10	0	0	0	20	10	70	90	0	0	0	0	10	16.2
GTxDMI	50	0	40	10	0	20	70	70	50	0	30	10	0	26.9
GTxAAO	0	0	0	20	10	0	30	60	40	0	0	0	10	13.1
Niño3xNiño4	50	10	10	50	0	20	30	70	0	10	10	60	0	24.6
Niño3xDMI	0	0	0	30	50	0	50	20	0	0	10	10	50	16.9
Niño3xAAO	10	0	20	40	0	70	60	100	0	0	20	20	0	17.9
Niño4xDMI	0	0	0	10	0	0	50	40	0	0	0	0	0	7.7
Niño4xAAO	0	0	0	10	0	10	40	40	0	0	0	0	0	7.7
DMIxAAO	0	0	10	10	0	0	80	70	30	0	10	0	0	16.2
Mean	15	16.5	18	30.5	18.5	38	62	74	25	15.5	15	24	18	28.5
Standard Dev	30	29.4	24.8	30.9	30.8	39.2	21.2	22.6	35.5	28.7	23.2	30.5	29.7	29.0
Skewness	1.81	1.79	1.92	1	1.56	0.61	0.24	-0.7	1.16	1.93	2.49	1.3	1.62	1.3
Kurtosis	1.79	1.87	3.59	-0.3	0.95	-1.4	-0.9	-0.3	-0.1	2.43	6.47	0.49	1.21	1.2

windows, none of the box portions overlap, suggesting significant warming. For the last two 20- year periods (1979-1998 versus 1999-2018), even the whisker portions do not overlap, suggesting a highly significant difference. To quantify the drying in the last two 20-year segments (1979-1998 versus 1999-2018), a permutation test was applied to the individual years, showing a warming of 0.855 °C and an associated a p-value of 0.001. The precipitation boxplots (Fig. 4) show that the first two 20-year segments have a higher mean, the second two 20-year periods show a marked decrease in precipitation and the last 20-year period is much drier. To quantify the drying in the last two 20-year segments (1979-1998 versus 1999-2018), a permutation test was applied to the individual years, showing a drying of 98.1 mm and an associated a p-value of 0.0087.

3.2. Wavelet analysis of Tmax and precipitation

The wavelet power spectra and global power spectra [10] for Tmax are shown in Fig. 5. Tmax does not exhibit a strong periodic influence. For Perth, the global power spectrum is minimal, and the wavelet power spectra shows

Table 2. Attribute selection for 13 different methods for precipitation prediction in Perth. The percent of folds selecting the attribute is shown for each of the 13 methods (columns 2-14). Statistics (mean, standard deviation, skewness and kurtosis) for each column is shown.

Attribute /Method	Cfs BF	LR BF	NN BF	SVR BF	RF BF	LR CS	NN CS	SVR CS	RF CS	LR Gr	NN Gr	SVR Gr	RF Gr	Mean
Global T	10	0	30	0	0	0	90	80	0	0	20	30	0	20.0
NPI	0	20	0	10	0	90	100	90	0	90	30	70	0	38.5
IPO	0	0	0	80	10	10	90	70	10	0	30	60	0	27.7
Niño3	0	0	10	30	90	10	60	80	90	0	30	40	50	37.7
Niño4	30	0	30	10	50	0	90	60	50	0	60	40	20	33.8
SOI	70	90	50	100	20	100	100	100	20	100	90	100	30	74.6
AMO	0	0	0	10	0	0	100	30	0	0	50	30	10	17.7
PDO	0	0	0	0	60	0	100	60	60	0	30	20	10	26.2
DMI	80	10	0	0	20	0	100	80	20	0	50	30	10	30.8
AAO	100	80	80	100	90	100	100	100	90	100	90	100	90	93.8
SSTA	100	20	10	0	0	30	100	60	0	30	10	70	0	33.1
GTxNiño3	0	10	0	0	20	0	60	40	20	0	10	10	40	16.2
GTxNiño4	0	0	0	0	0	0	80	30	0	0	20	10	10	11.5
GTxDMI	90	0	10	10	0	0	70	90	0	0	60	60	0	30.0
GTxAAO	0	0	10	0	10	0	90	40	10	0	20	10	10	15.4
Niño3xNiño4	0	0	0	0	10	0	70	50	10	0	0	20	10	13.1
Niño3xDMI	80	30	0	70	20	0	80	60	20	0	30	20	10	32.3
Niño3xAAO	0	0	0	0	40	30	80	80	40	30	40	60	20	32.3
Niño4xDMI	0	0	20	0	10	0	70	80	10	0	10	30	0	17.7

Niño4xAAO	0	10	10	10	50	30	80	80	50	30	50	60	10	36.2
DMIxAAO	0	0	20	0	10	50	100	90	10	50	60	60	0	34.6
Mean	26.7	12.9	13.3	20.5	24.3	21.4	86.2	69.0	24.3	20.5	37.6	44.3	15.7	32.1
Standard Dev	39.9	25.5	24.8	34.6	28.4	34.5	14.0	21.7	28.4	35.0	24.9	27.3	21.8	27.8
Skewness	0.92	2.22	1.92	1.50	1.20	1.45	-0.5	-0.4	1.20	1.46	0.62	0.55	2.12	1.1
Kurtosis	-1.0	1.87	3.62	0.52	0.25	0.57	-1.1	-1.0	0.25	0.55	-0.4	-0.7	4.22	0.6

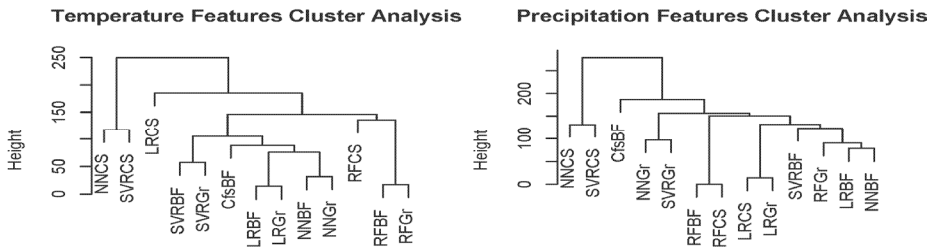

Fig. 2. Dendrograms of average linkage cluster analysis of attribute selection methods for temperature (left panel) and precipitation (right panel).

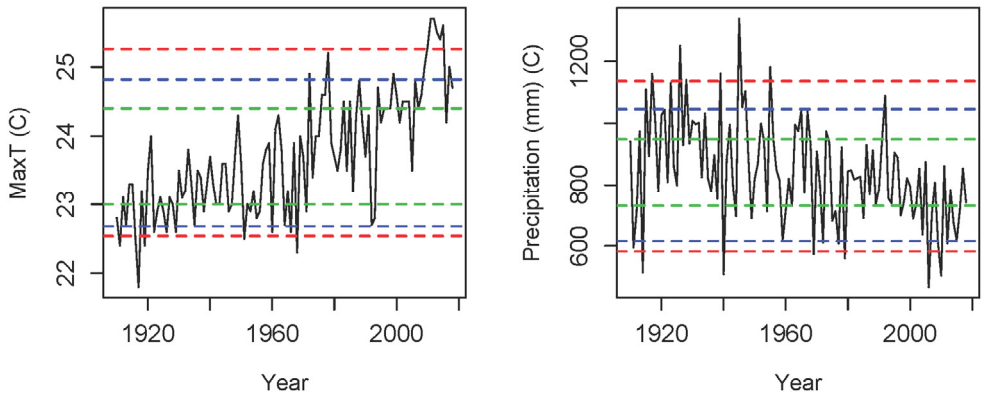

Fig. 3. Time series of annual maximum average temperature (left) and annual total precipitation (right) for Perth. Percentiles (25/75, 10/90 and 5/95) are shown as green, blue and red dashed lines, respectively.

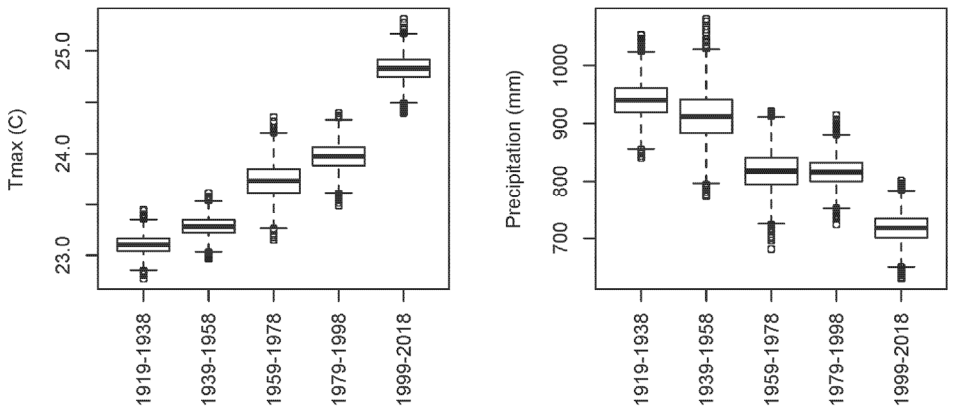

Fig. 4. Boxplots of 5000 bootstrap replicates of 20 years periods of annual maximum average temperature (left panel) and annual total precipitation (right) for Perth.

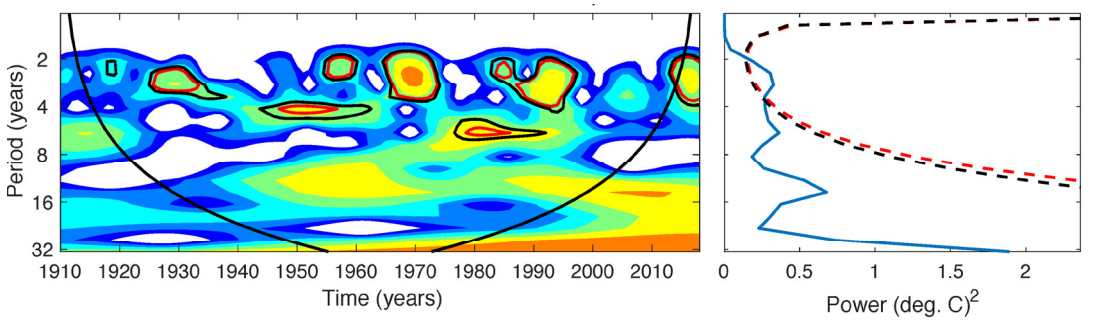

Fig. 5. Perth Tmax time wavelet analysis. Left panel shows the local spectra. Right panel shows the global spectra.

a 2 to 8-yr periodic signal at both the 90th and 95th confidence levels. For the precipitation data, Fig. 6 shows both the wavelet power spectra and global power spectra with a clear 2 to 4-year periodicity, which is highly suggestive of an El Niño/Southern Oscillation signals, known as ENSO (hence the Niño3, Niño4 and SOI predictors were included). However, it appears the ENSO signal became weaker and occupied shorter periods of time in Perth, from the 1980s onwards. A second, longer term, periodic signal is present in Perth over a 16 to 32-yr period, though this second periodic signal is not statistically significant at the 95% confidence level, it is sufficiently strong to have a possible influence on recorded precipitation.

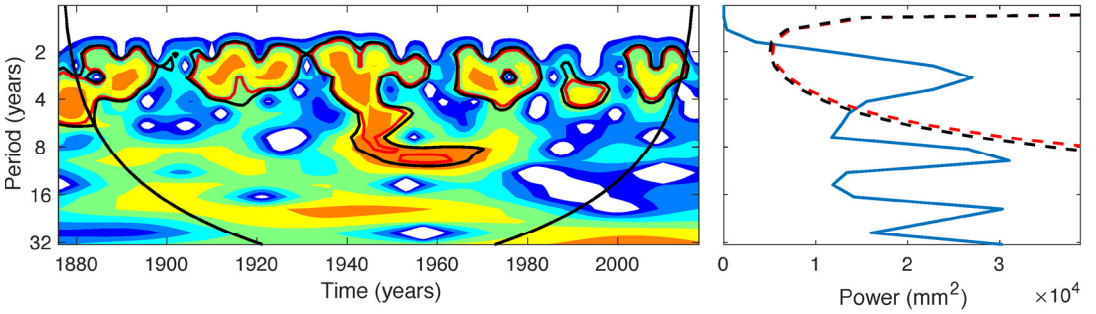

Fig. 6. Perth precipitation wavelet analysis. Left panel shows the local spectra. Right panel shows the global spectra.

3.3. Statistical and machine learning prediction of Tmax and precipitation in Perth

Four methods were employed for prediction: a linear multiple regression served as a baseline, a backpropagation neural network with a single hidden layer, a support vector regression with a polynomial kernel and a random forest. Data for the period 1910 to 1981 (66.6 percent) served as training data for further attribute selection and cross-validation to fit model parameters and the 1982 to 2018 data (33.3 percent) served as testing data. In each of these methods, the attributes selected in Tables 1 and 2 were used as a starting point. An attribute withholding was applied, noting both the correlation and root mean squared error (RMSE) between the predicted and observed testing data in a 10-fold cross-validation. The most parsimonious model with the highest correlation and lowest RMSE was selected. That model was used to predict the testing data and the model performance was documented.

For Tmax, the linear regression model that performed best contained the attributes GlobalT, Niño4 and DMI. NN uses the same attributes as LR, whereas SVR uses GlobalT, PDO and DMI. RF uses GlobalT and DMI. For the precipitation predictions, LR uses NPI, SOI and AAO, NN uses SOI and AAO, SVM uses IPO, SOI, AAO, Niño4xAAO and DMIxAAO and RF uses PDO and AAO. precipitation, the linear regression model that performed best contained the attributes NPI, SOI and AAO. NN uses SOI and AAO. SVM uses IPO, SOI, AAO, Niño4xAAO and DMIxAAO. RF uses PDO and AAO. Using correlation between the observed versus predicted precipitation testing data as the arbiter, the ranking of the models from most to least accurate was: SVR, LR, NN and RF (for Tmax, Table 3) and SVR, LR, NN, RF (for precipitation, Table 3). The histograms of the errors corresponding to Table 3 are shown in Fig.7a-d, which shows the bias and predisposition of the errors. In contrast with the correlation between observed and predicted, the RMSE values differed in the ranking order of the least accurate models: LR, SVR, NN and RF for Tmax (Table 3) SVR, LR, RF, NN for precipitation (Table 3). Again, the histograms of the precipitation errors are shown in Fig. 7e-h. The reason for the difference between observed and predicted Tmax (Table 3; Fig. 7b) was that the NN model failed to extract the decreasing precipitation trend. This is a known property of NNs [11] and can be addressed through detrending or adopting a more complicated ARIMA approach. However, in a true forecasting situation, the trend is not known. Similarly, the RF failed to capture the upward trend in Tmax. Interestingly, the RF model predicted the trend best for precipitation but failed to capture the upward trend in Tmax as

seen in the large negative mean error (Table 3). RF failed to capture the year-to-year precipitation variability as accurately as the SVR or LR models, as seen in the smallest correlations and larger RMSE , though NN had the largest RMSE (Table 3).

Table 3. Performance of Tmax and precipitation (Pr) models on testing data. Tmax (columns 2-5) and Pr (columns 6-9).

Model	Tmax LR	Tmax NN	Tmax SVR	Tmax RF	Pr LR	Pr NN	Pr SVR	Pr RF
Correlation	0.686	0.655	0.694	0.301	0.488	0.480	0.537	0.411
RMSE (°C)	0.53	0.54	0.54	0.98	111.8	135.4	103.9	122.2
Error Mean (°C)	0.05	0.00	-0.16	-0.70	-23.3	71.6	4.7	41.8
Error SD (°C)	0.43	0.55	0.53	0.69	110.8	116.6	105.2	116.4
Error Skewness	0.21	0.11	0.23	0.29	0.10	0.18	0.68	0.24
Error Kurtosis	-0.65	-0.58	-0.76	0.08	-0.16	0.57	0.42	-0.29

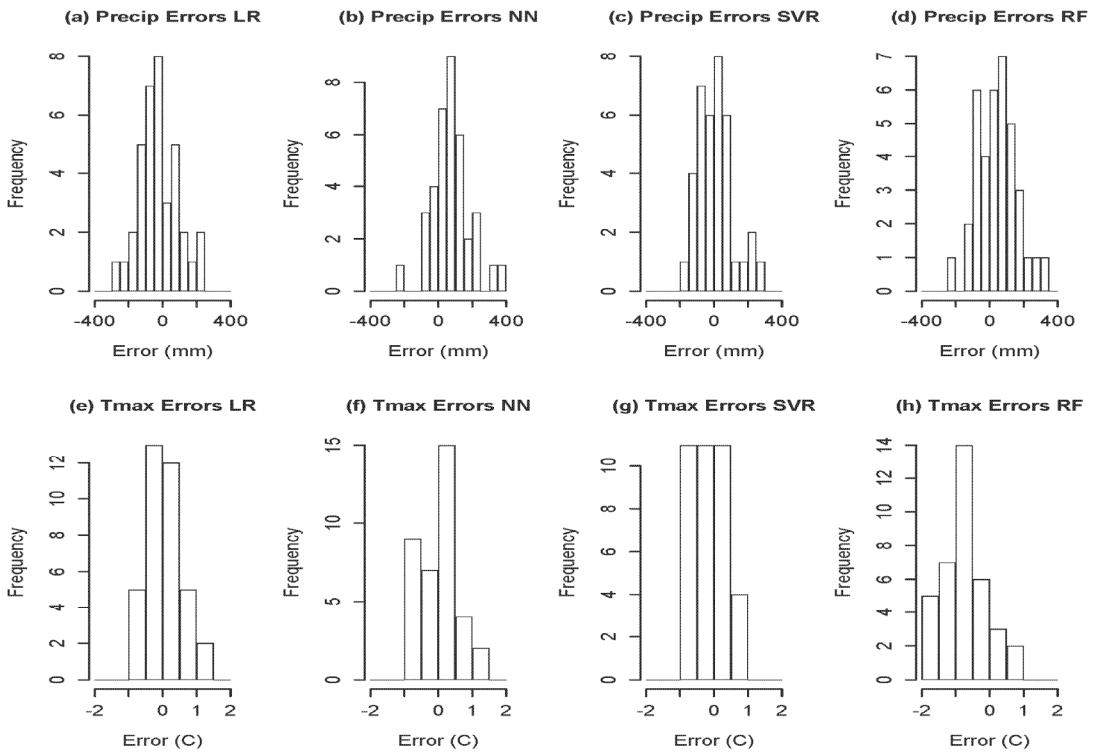

Fig. 7. Histograms of the precipitation and maximum temperature forecast errors for the testing data. Panels (a-d) are precipitation errors for LR, NN, SVR and RF, respectively. Panels (e-h) are temperature errors for R, NN, SVR and RF, respectively.

4. Conclusions

The recent water supply issues in other global cities motivated this study of one of Australia's most vulnerable cities, Perth, which is located in southwestern Australia, at a similar latitude to Cape Town and southern California

and with a similar, Mediterranean climate. Detailed statistical analysis confirmed a significant decrease in wet season rainfall (98.1 mm decrease in the past two 20-years periods) and increasingly warming maximum temperatures (Tmax) of 0.855 °C, over those same periods. These are highly significant changes that were measured by permutation test p-values of 0.0087 and 0.001, respectively. This combination of drying and heating, coupled with increased demand from a growing population trend is of great importance for water supply policies and management as over 4 billion people live in the subtropical and tropical regions experiencing increasingly hot and a drying climate.

Using the observed time series of precipitation and maximum temperatures a search was carried out for the possible atmospheric and oceanographic attributes, especially for the dramatic trends in both maximum temperature (warming) and precipitation (drying). Using long-length datasets of oceanic and atmospheric climate drivers (including a global warming driver) that spanned 1910 to 2018. These attributes and the targets (temperature, precipitation) were divided into a training set (1910-1981) and a testing set (1982-2018). The training set was subject to a suite of attribute selection methods. The wavelet analysis of the maximum temperature did not show any statistically significant periodicities; however, the precipitation data exhibited significant power in the global spectra between 2 and 8 years, suggesting some El Niño/Southern Oscillation influence. Results of that selection process suggested that only 2 to 5 attributes were necessary to fit a LR, NN, SVR and a RF model that generalized well to the testing data. In the case of Tmax, the highest predictive correlations were SVR, LR and NN which all were above 0.65, with RF trailing at 0.301. For precipitation, all of the correlations were moderate, ranging from 0.411 to 0.537 with SVR the best-performed, followed by LR, NN and RF. For temperature, the three best performing models were statistically indistinguishable in RMSE; however, RF had a significantly larger RMSE. For precipitation, both SVR and LR had the smallest RMSE, followed by RF and NN. NN often had prediction errors (Fig. 7) larger than the other methods, despite investigation of a range of NN hyperparameters on the training data. This suggests some relationships among the training data attributes are changing as the climate changes (i.e., testing data), casting some doubt on the validity of using NN to processes historical data relations to create accurate future predictions for these precipitation data.

Acknowledgements

This study was supported by funding from the School of Mathematics and Physical Sciences, University of Technology Sydney.

References

[1] Richman, M.B. and L.M. Leslie. (2018) “The 2015-2017 Cape Town drought: classification and attribution using machine learning”. *Procedia Computer Science* **140**: 248–257.

[2] Ramsey, H.A., M.B. Richman and L.M. Leslie. (2014) “Seasonal tropical cyclone predictions using optimized combinations of ENSO regions: application to the Coral Sea basin”. *J. Climate* **27**: 8527-8542.

[3] Richman, M.B., L.M. Leslie, H. Mansouri and T.B. Trafalis. (2014) “Data selection using support vector regression”. *Adv. in Atmos. Res.* **32:** 277-286.

[4] Pasini, A., P. Racca, S. Amendola, G. Cartocci and C. Cassardo. (2017) “Attribution of recent temperature behaviour reassessed by a neural network method”. *Scientific Reports.* **7:** 17681.

[5] Naing, W.Y.N and Z.Z. Htike. (2015) “Forecasting of monthly temperature variations using random forests”. *ARPN J. of Engineering and Applied Sci.***10:** 10109-10112.

[6] Hall, M.A. (1998) “Correlation-based Feature Subset Selection for Machine Learning.” PhD dissertation. Hamilton, New Zealand.

[7] Kohavi, R. and G.H. John. (1997) “Wrappers for feature subset selection.” *Artificial Intelligence*. **97(1-2)**:273-324.

[8] Mendialdua I., A. Arruti , E. Jauregi, E. Lazkano and B. Sierra. (2015) “Classifier subset selection to construct multi-classifiers by means of estimation of distribution algorithms.” *Neurocomputing*. **157**:46–60

[9] Caruana, R. and D. Freitag. (1994) “Greedy attribute selection”, *Machine Learning Proceedings.* 28-36.

[10] Hartigan, J., S. MacNamara and L.M. Leslie. (2019) “Comparing temperature and precipitation trends between inland and coastal locations”. *ANZIAM J.* **60**: C109-C126.

[11] Zhang, P.G. and M. Qi. (2005) “Neural network forecasting for seasonal and trend time series.” *European J. of Operat. Res.*, **160,** 501-514.